Yelita

RELATIVE METROLOGY GAUGE

- The linear relative metrology gauge had reached an accuracy of 0.15 pm rms in vacuum. This meets the OSI linear gauge requirement.

- O The accuracy mentioned above was obtained by comparing two independent gauges monitoring the distance between two corner cubes.

- Small changes in the temperature (few millidegrees) cause the two interferometers to go out of alignment with respect to each other producing a linear drift between the two gauge readings (< 10 pm rms per measurement).

- O A dithering mechanism which moves the beam launcher to find the optimum alignment position has been developed. The complete gauge will be tested this summer.

Insert after page L1. Cover page # = 1.

SURFACE METROLOGY ALGORITHM

CCD images:

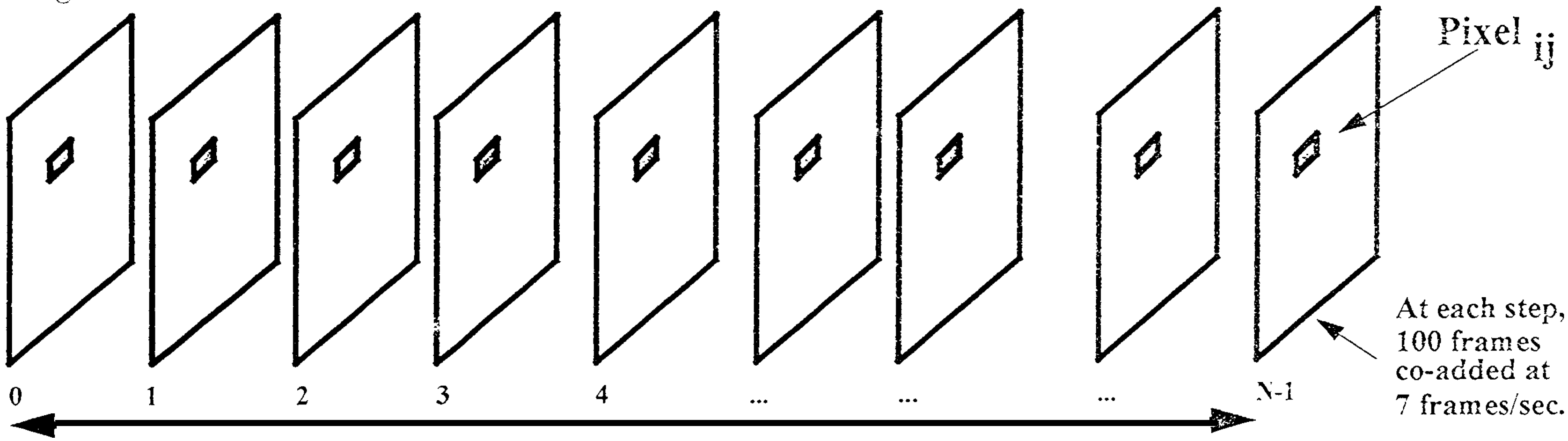

N pzt steps

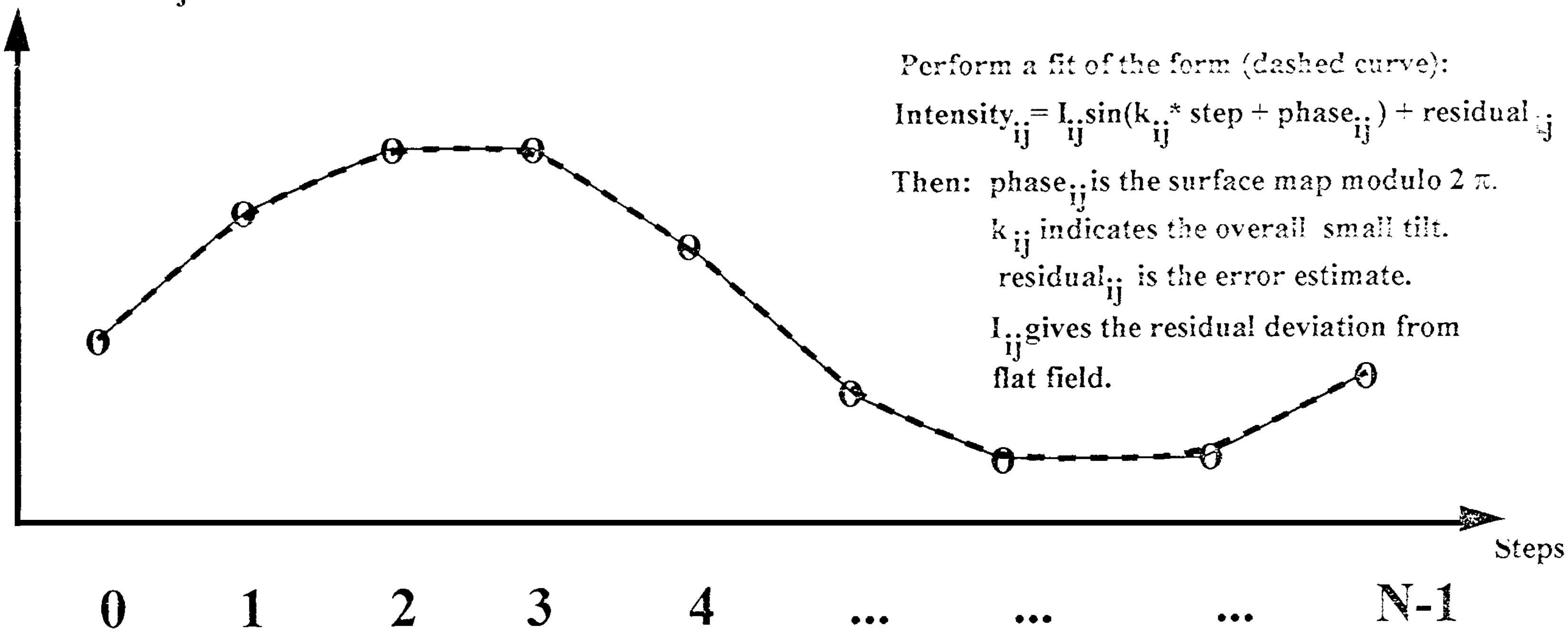

Perform a fit of the form (dashed curve):

$\text{Intensity}_{ij} = I_{ij} \sin(k_{ij} * \text{step} + \text{phase}_{ij}) + \text{residual}_{ij}$

Then: phase_{ij} is the surface map modulo 2π.

k_{ij} indicates the overall small tilt.

residual_{ij} is the error estimate.

I_{ij} gives the residual deviation from flat field.

Yelita

LASER FREQUENCY STABILIZATION SCHEME

With narrow frequency modulation and utilizing the magnitude of the reflection coefficient

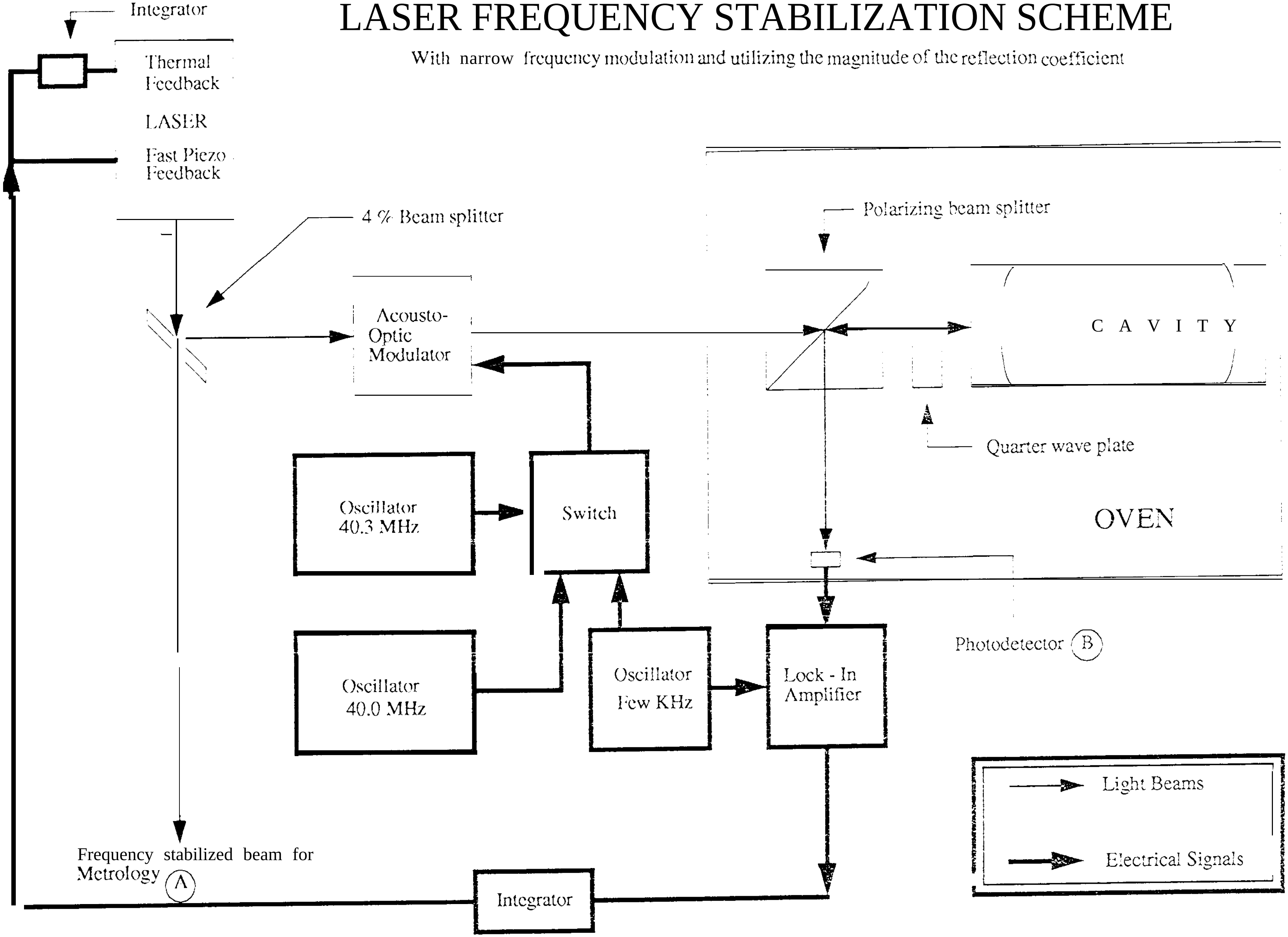

M e for spatial interferometry

Yekta Gürsel

Jet Propulsion Laboratory
California Institute of Technology
4800 Oak Grove Dr., Pasadena, CA 91

ABSTRACT

Very high resolution spatial interferometry requires picometer level one-dimensional metrology, surface metrology and 3-dimensional metrology. Micron level accuracy is required for absolute metrology systems for spacecraft like the proposed Orbiting Stellar Interferometer (OSI) carrying high resolution spatial interferometers.

A surface metrology system with a repeatability of less than 0.1 nm over an aperture of several nches in vacuum has been demonstrated. An absolute calibration system for this gauge is in development.

An absolute metrology system with an accuracy of 10 microns over a distance of 10 meters is also under construction. This system uses a 1319 nm, solid-state, infrared laser locked to an Ultra-Low-Expansion (ULE) glass cavity to an accuracy exceeding 1 part in 10^{10}. The length of the cavity is controlled by a thermal vacuum oven. 1 millidegree Centigrade root-mean-squared (rms) cavity temperature stability with the oven in vacuum has been achieved for time scales of days. The digital laser servo is capable of following the length of the cavity with an Allen deviation of few hundred Hertz for time scales of a day. Two lasers locked to the same cavity are used to supply a simultaneous cavity length measurement as well as the absolute distance measurement. The absolute distance measuring part of the gauge is under construction.

An auto alignment system is being developed for our linear relative metrology gauge which had achieved an accuracy of 0.1 picometers. This gauge will be used to construct a 3-dimensional metrology gauge with an accuracy of less than 10 pm rms for time scales of minutes initially.

1 INTROI UCTION

Very high resolution spatial interferometry requires picometer level one-dimensional metrology, surface metrology and 3-dimensional metrology. Micron level accuracy is required for absolute metrology systems for spacecraft like the Orbiting Stellar Interferometer (OSI) carrying high resolution spatial interferometers.

In two previous papers[1,2], we demonstrated an accuracy of 0.15 picometers root-mean-squared (rms) for the Orbiting Stellar Interferometer (OSI) relative metrology gauge. This accuracy was obtained by comparing two independent gauges monitoring the distance between two corner cubes. Small changes of the order of few millidegrees Centigrade in the temperature cause the two interferometers to go out of alignment with respect to each other producing a linear drift between the two gauge readings. This linear drift is few picometers rms in magnitude.

To remove this linear drift, a dithering mechanism which moves the beam launcher cube during the measurement has been developed. The position of optimum alignment for each interferometer can be deduced from the dithered data. This method of drift removal will be tested early this summer. The resulting drift free, picometer accuracy linear metrology gauge will be used in constructing a 3-dimensional metrology gauge with less than 10 picometer rms accuracy

The remaining two gauges, namely the surface metrology gauge and the absolute metrology gauge, are nearly complete. In what follows, I will give a detailed description of the surface metrology gauge and the absolute metrology gauge with their current performances. The design for the 3-dimensional gauge is presented afterwards.

Figure 1: The surface metrology gauge

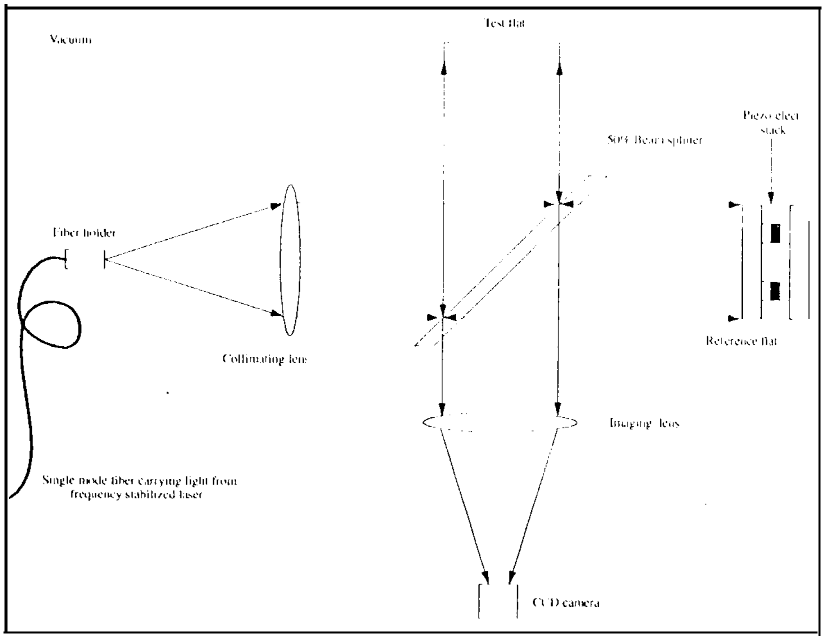

2 SURFACE METROLOGY GAUGE

2.1. Gauge Description

The basic gauge architecture is shown in Fig. 1. A stabilized, polarized Helium-Neon laser is coupled into a polarization preserving fiber. The fiber goes through a vacuum seal and enters the four feet vacuum chamber. It is attached to a fiber holder with three degrees of freedom. The fiber holder and the rest of the gauge is attached to a 3' by 4' by 2" optical breadboard. The breadboard rests on vibration isolating, silicone rubber pads attached to the skin of the vacuum chamber. The chamber itself rests on four pneumatic vibration isolators.

On the breadboard, an anti-reflection coated, low-aberration, collimating lens assembly creates a nearly afocal beam with a diameter of three inches. A four-inch clear aperture, $\lambda/20$ flatness, 50%-50% beam splitter separates the beam into two equal intensity beams forming a Michelson interferometer.

One of the beams reflects from a 2" reference flat which is mounted on a three degree of freedom stage. T stage supplies the tip, the tilt and the rotation-about-the-axis-of-the-beam degrees of freedom.

The other beam reflects from a 2" test flat which is mounted on another three degree of freedom stage that supplies the coarse and fine tip, the coarse and fine tilt and the piston degrees of freedom.

The two reflected beams are combined together at the beam splitter to form the interference fringes. An imaging lens images both of the mirrors on an uncooled, 8-bit commercial CCD video camera forming an equal arm interferometer within the depth of focus of the optical system. The optical system is aligned to give zero bias fringes across the whole field of view.

The output of the camera is brought out of the chamber through a vacuum feedthrough and it is digitized by a frame grabber on a VME bus computer system.

The computer system steps the piston piezo-electric transducer and collects data at each step, co-adding images pixel by pixel to improve the signal-to-noise ratio. The resulting set of images are written to magnetic disk for subsequent analysis.

Figure 2: The surface metrology algorithm

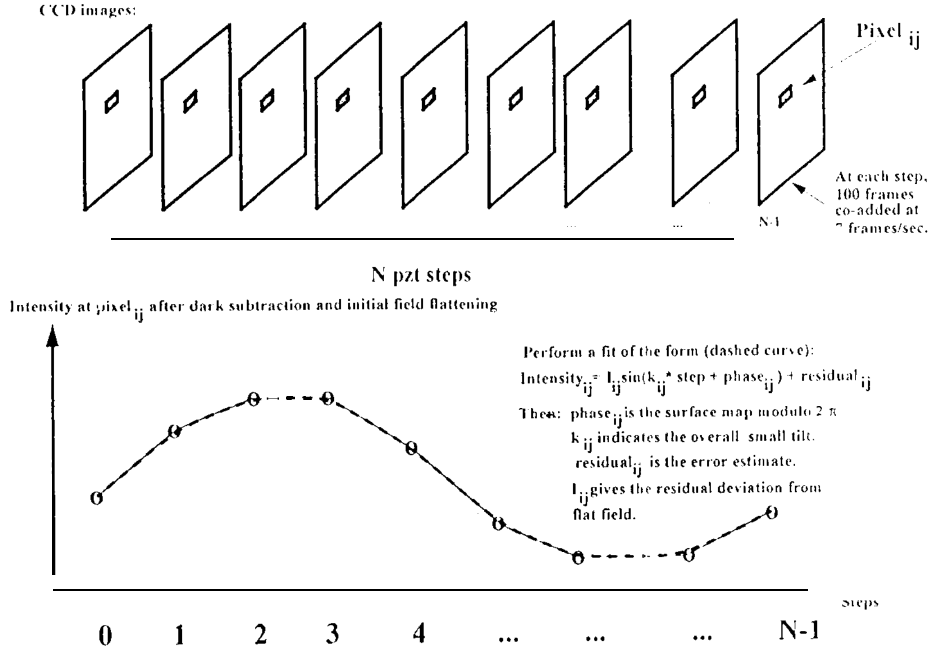

2.2. Measurement Procedure

In the actual measurement, a wavelength is divided in 80 nearly equa parts. The piston ransducer is stepped through two wavelengths, pausing to collect data at each step.

One hundred video frames at a resolution of 320 by 240 pixels are co-added pixel by pixel at the rate of 7 frames per second by the stepping CPU to create a single image at each step. This improved image is stored on magnetic disk before proceeding to the next step. The measurement phase ends when the stepping CPU collects 160 enhanced images corresponding to the steps in the two-wavelength scan. A final enhanced dark image with the measurement laser blocked is taken to calibrate the dark level for the measurement.

2.3. Analysis Procedure

The data analysis is performed off-line by a faster computer as illustrated by Fig. 2. The algorithm considers each pixel independently and it is completely parallel suitable for multi-processor systems.

First, dark image subtraction is applied to all of the images to set the zero-intensity level. Then, a "flat-field" image is generated by adding all images which span almost exactly a wavelength. All of the images are then dynamic range compensated using this "flat-field" image.

The surface figure extraction for each pixel proceeds as follows: A cross-section of the intensity across all the images corresponding to the pixel considered is constructed as a function of the step number. Ideally, this is a simple sinusoidal curve with constant amplitude, frequency, phase and offset. The actual measurement is contaminated with noise, so a non-linear, least squares fit is performed with the amplitude, the frequency, the phase and the offset as parameters. The initial values for the fit is generated by considering global changes across the curve.

The phase thus obtained gives the "disconnected" phase across the surface. Since there are zero bias fringes across, and the mirrors are nearly flat, the "disconnected" phase can only be different from the neighboring pixels by multiples of 2π. After every pixel is processed, a scan across the phase map is performed to match all phases to the first pixel of the image using the continuity of the phase across the image. The actual surface figure is directly proportional to the phase map. A phase difference of 4π corresponds to a change in flatness by one wavelength of the ase. light

"

Figure 3: Phase image without spurious fringe rejection

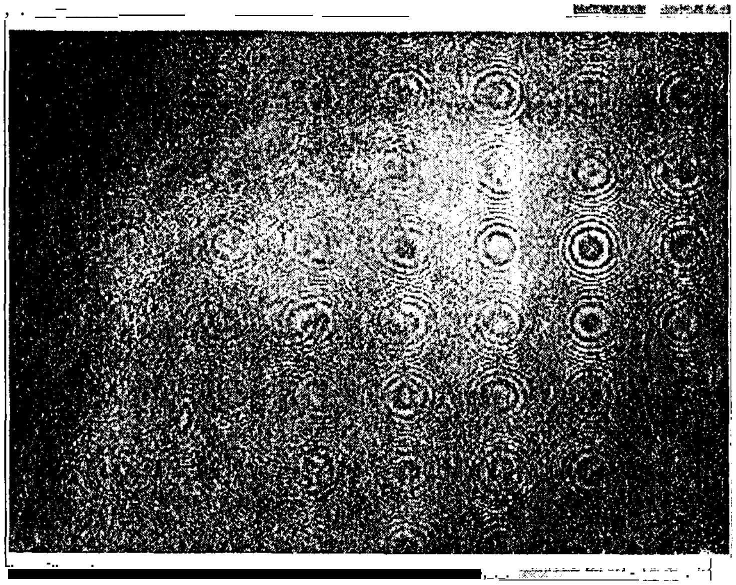

The other derived parameters give indications of the goodness of the algorithm. The amplitude image is a measure of the quality of the flat field compensation. The frequency image informs about the wobble of the piston transducer as it pushes the test flat. The offset image is a measure of the quality of the dark compensation. The "chi-square" image which is formed by the "chi-square" values for each pixel fit tells whether the fits across the image are of the same quality.

2.4. Systematic Errors

Systematic errors arise due to spurious reflections in the optical system finding their way into the CCD camera. These spurious fringes move with the residual vibrations leaking through the isolation system. Since many images are added at each piston transducer step, the motion of the spurious fringes are registered differently by each enhanced image. The common part of the spurious fringes which stays the same in each enhanced image is cancelled by the non-linear fit procedure. The moving part of the spurious fringes is not cancelled and it appears as a systematic error in the measurement result.

In order to eliminate these systematic errors, the entire CCD camera is mounted on an axial motion stage which moves by many wavelengths of the laser light perpendicular to the beam during the exposures. This motion is well within the depth of focus of the system and it does not cause loss of image resolution. It completely removes the systematic errors due to spurious fringes since they are periodic with the wavelength of the laser light.

Fig. 3 and Fig. 4 illustrate the results of the spurious fringe removal procedure. Fig. 3 shows a phase image with stationary camera. There are many spurious fringes arranged regularly across the image. These are caused by the back- reflected light from the CCD camera and they are indeed fringes representing the pixels of the camera enlarged by the optical system. Fig. 4 shows the result of the subsequent measurement with the moving CCD camera. All spurious fringes have been eliminated by this procedure.

No optical system aberration errors appear in the results since both of the beams follow exactly the same path through the optical system. Hence, making a large aperture surface metrology system involves only purchasing large diameter collimating and imaging lenses and a large diameter beam splitter. The rest of the system functions as built.

Another source of systematic errors is the temperature drift during the measurements. Two subsequent mea-

Figure 4: Phase image with spurious fringe rejection

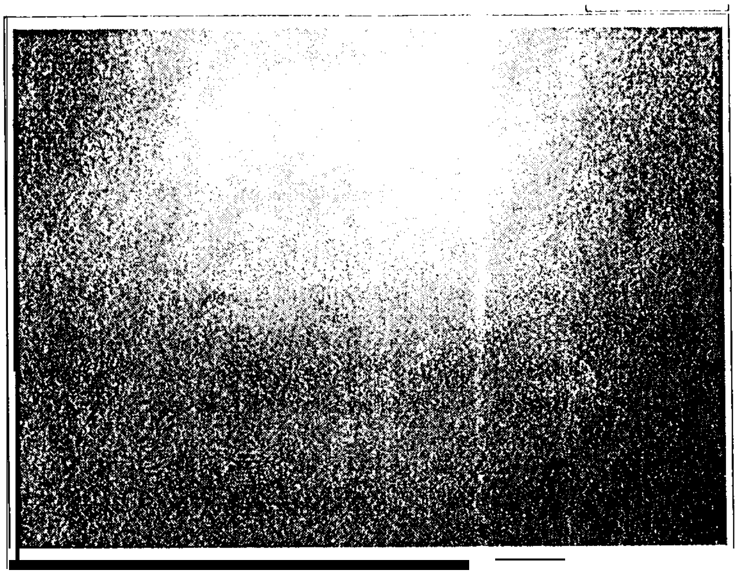

surements may not agree since in the intervening time, one or both of the mirrors may have been warped due to the fluctuating temperature. These effects are not noticed at the $\lambda/100$ level of resolution where λ is the wavelength of the laser light. However, they are well pronounced at the $\lambda/1000$ level of resolution. To eliminate such errors while comparing measurements, the exposures for the corresponding measurements are interleaved. An absolute measurement device has to be actively temperature stabilized to sufficient accuracy to prevent warping due to fluctuating temperature. This may require special mounts for the reference and the test optics.

The remaining sources of systematic errors are the reference flat and the beamsplitter. All measurements are performed with respect to a fixed orientation of the reference flat and the beamsplitter. An algorithm which eliminates the reference flat figure and the beamsplitter figure from the measurements is under development.

2.5. Measurement Results

The figures Fig. 5, Fig. 6, Fig. 7, Fig. 8, Fig. 9, Fig. 10 show some of the results obtained using the surface metrology gauge. First five figures are the results of two interleaved runs with 100 frames co-added at each step over a wavelength. Each runs consists of 80 steps over a wavelength of piston transducer motion.

Fig. 5 shows the surface figure error of two 2" flats (reference and test) in measurement run (a). Each of these mirrors are rated at $\lambda/10$ by their manufacturer. The figure covers the central 1" square of the mirrors.

Fig. 6 shows the surface figure error of two 2" flats (reference and test) in measurement run (b). Each of these mirrors are rated at $\lambda/10$ by their manufacturer. The figure covers the central 1" square of the mirrors.

Fig. 7 shows the difference between the two runs. The rms figure error is nearly $\lambda/6,000$. The following two figures show the difference between the two runs analyzed in a different way to reveal the instrument noise level and the effects of temperature drifts. One of the runs is taken to be the sum of the two runs: All images taken in the measurements are considered to be a single run. Then, the individual runs are subtracted from it.

Fig. 8 shows the difference between the phase result of run (a+b) and run (a) while Fig. 9 shows the difference between the phase result of (a+b) and run (b). In the first case the rms figure error improved significantly. The next case reveals an upper bound for the instrument noise level including the fit error: It is nearly $\lambda/60,000$ rms in the large flat region which almost entirely covers the figure.

The figure Fig. 10 shows the results of a test run with 25 frames co added at each piston transducer step.

Figure 5: Surface figure error as measured by run (a)

Deviation From Flatness (09/02/940)

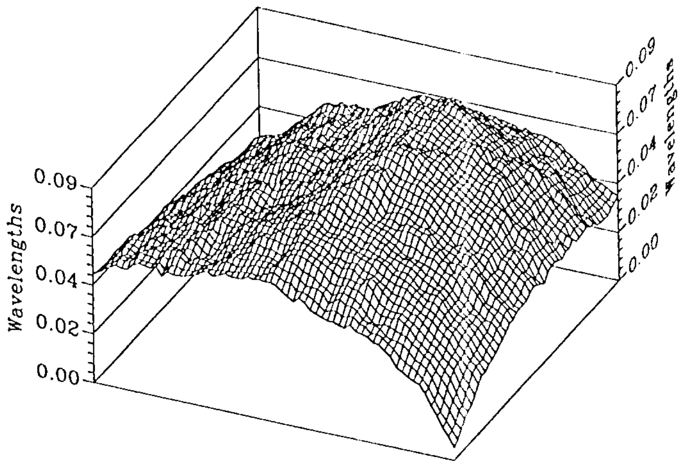

F'– V error: 0.08838 Rms error: 0.01551

Figure 6: Surface figure error as measured by run (b)

Deviation From Flatness (09/02/94b)

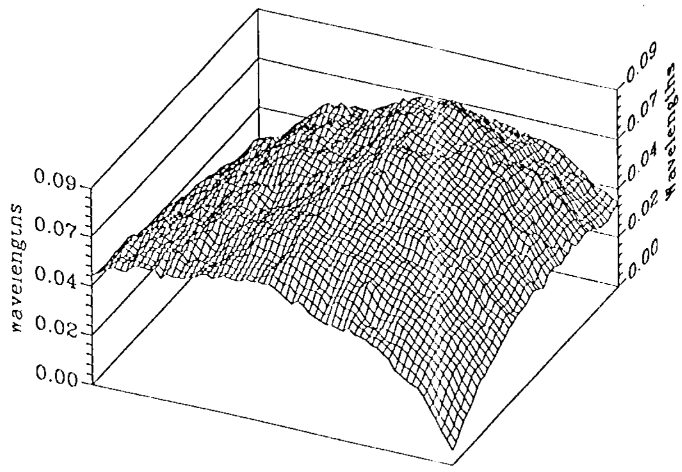

P–V error: 0.08916 Rms error: 0.01563

Figure 7: The difference between the two runs: (b) -(a)

Repeatability (09/02/94b – 09/02/94a)

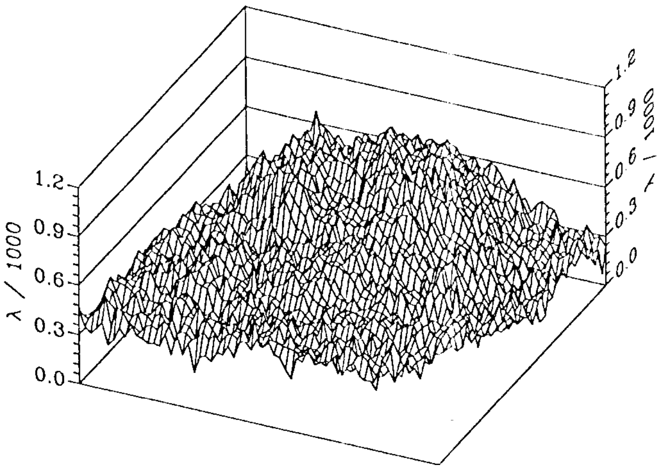

P-V error: 1.229 Rms error: 0.1 849

Figure 8: The difference between the two runs: (a+b) -(a)

Repeatability (09/02/94 a+b - 09/02 /94a)

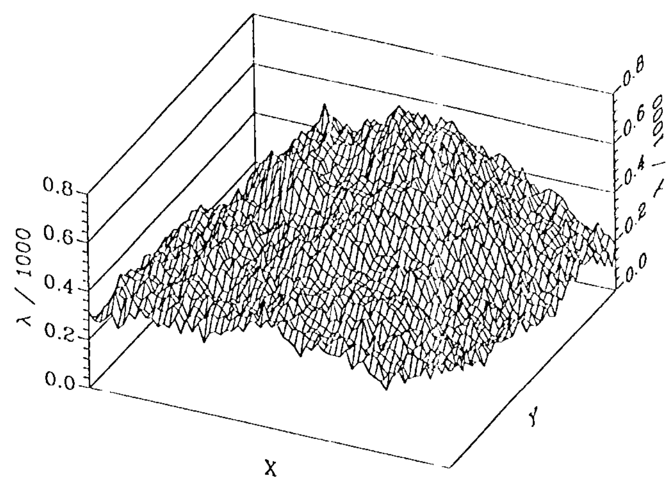

P–V error: 0.8375 Rms error: 0.15134

'igure 9: The difference between the two runs: (a+b) - (b)

Repeatability (09/02/94 a+b - 09/02/94b)

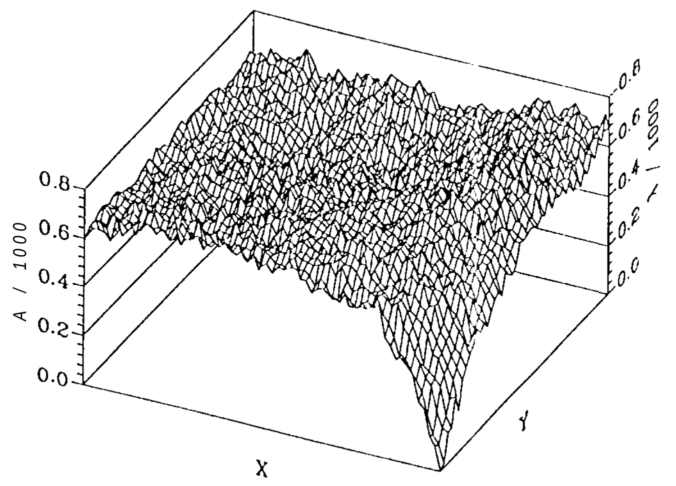

P–V error: 0.8232 Rms error: 0.07576

The number of steps was equal to the the number used in the measurements above. The difference between two interleaved test runs is shown to indicate the photon noise level. There is no appreciable difference between the results of this run with reduced co-added frame number and the runs with four times larger co-added frame number. This fact alone cuts the measurement time by a factor of four also reducing the effects of temperature drifts.

Further results demonstra ing the reference mirror figure and the beamsplitter figure subtraction together with improved measurement speed and thermal response will be described in a subsequent paper.

3. AI SOLUTE METROLOGY GAU GE

The dual infrared laser absolute metrology gauge consists of three parts: The dual laser stabilization system with cavity length readout, the heterodyne modulation system and the absolute and relative distance monitor. In what follows, I will describe the basic gauge architecture, the laser stabilization technique, the measurement technique, and the detailed performance of gauge subsystems.

3.1 Gauge Description

The absolute metrology gauge laser stabilization system is shown in Fig. 11. Two 1319 nm, solid state, diode pumped lasers are coupled to polarization preserving fibers with two separate outputs. The low power outputs ($\sim$ 1mW) are modulated at two different frequencies and combined together with a 50%-50% fiber coupler. The combined light is routed to a vacuum thermal oven which contains a ULE Fabry-Perot cavity.

The Fabry-Perot cavity consists of a 5 cm long spacer optically contacted to two 10 cm radius of curvature spherical mirrors. The fringe width of the cavity is 300 kHz which is determined by the mirror coatings. The cavity is suspended in a cylindrical copper canister with two perpendicular delrin spiders which prevent the cavity from tilting with respect to the axis of the canister. One end of the cavity can slide in the holder to prevent the spiders from pulling the cavity as the thermal oven is heated to the operating temperature.

The copper canister itself is suspended from a three-rod optical bench with two perpendicular delrin spiders. Three heating pads and a thermistor on the canister form the transducers and the sensor of the cavity heater servo.

The infrared laser light reaches the cavity after passing through the skin of the vacuum chamber in a polarization

Figure 10: The repeatability with reduced co-adding number

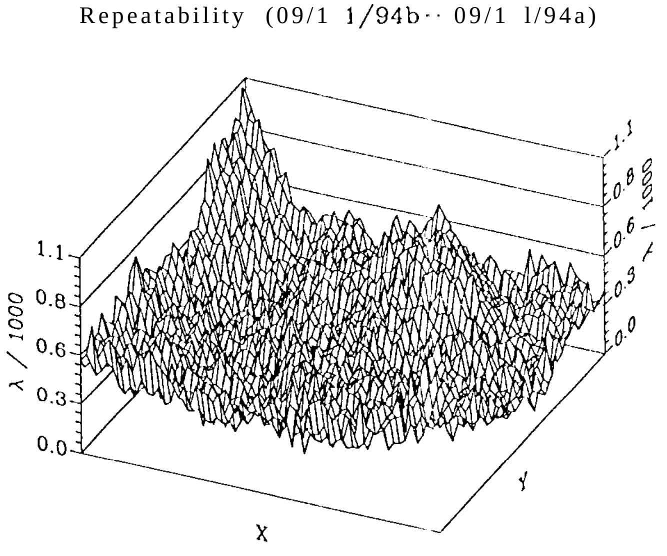

P-V error: 1.112 Rms error: 0.1513

Figure 11: The absolute metrology gauge stabilization system

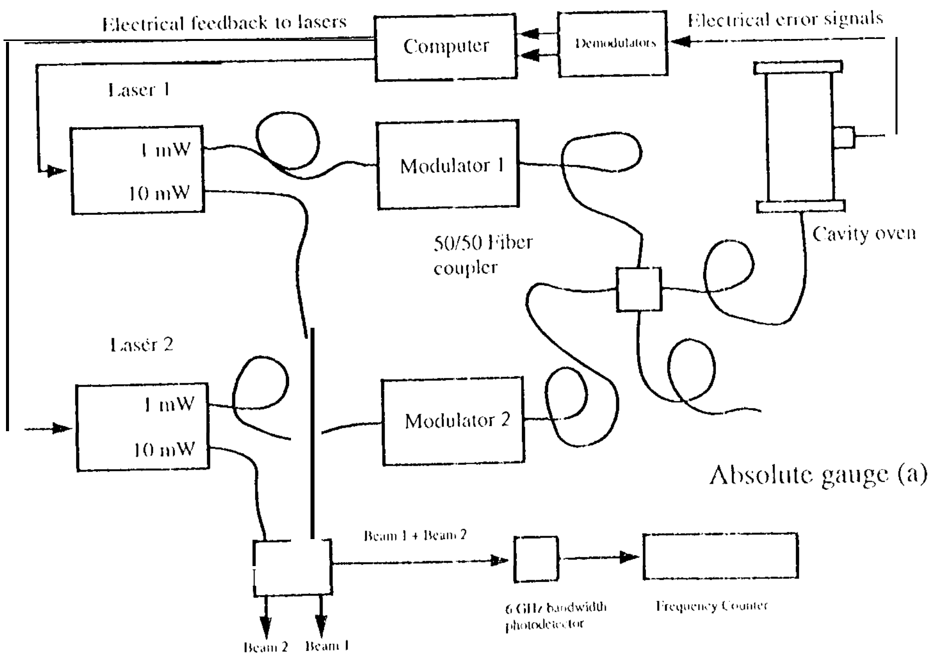

Figure 12: The absolute metrology gauge heterodyne modulation system

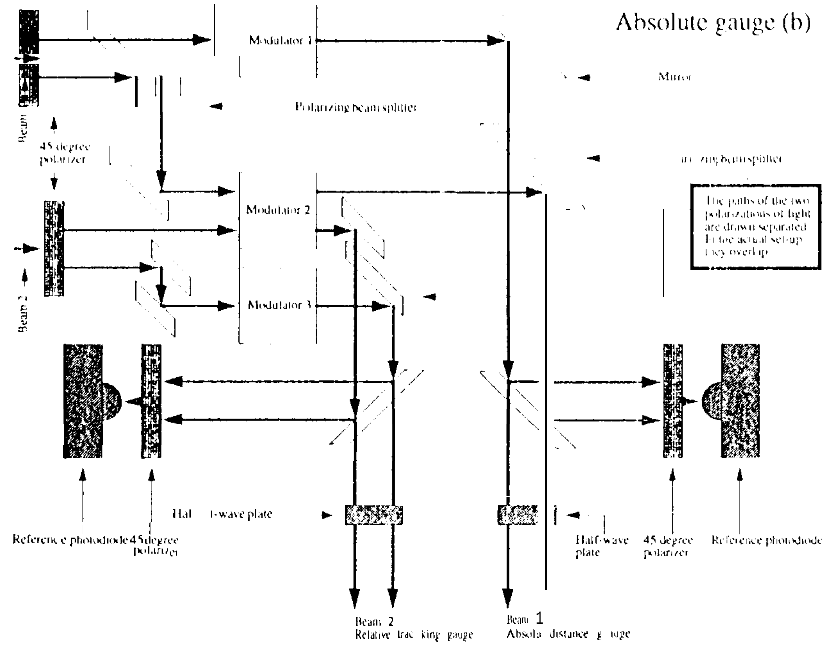

preserving fiber in a vacuum feedthrough. The light from the fiber is mode-matched to the cavity by a singlet lens and reaches the cavity through an axial hole in the copper canister after passing through a polarization circulator just outside the canister. The light reflected from the cavity is diverted by the polarization circulator to a photodetector which also resides in the vacuum chamber near the copper canister.

The vacuum chamber is a 4" inner diameter, 12" long conflat vacuum nipple. The laser light aligned with respect to the cavity in such a way to make the TEM_{00} mode of the cavity to carry most of the incoming energy when the frequency of the input light matches the resonance frequency of the mode. The alignment is performed once when the chamber is open. It stays fixed and untouched after the vacuum chamber is closed.

The electrical signals from the photodetector inside the chamber are brought out by a vacuum feedthrough and they are demodulated by an array of demodulators. The outputs of the demodulators are separately digitized by a 16 bit, multi-channel A/D. A single board computer computes the servo feedback signals and drives the piezo-electric and the thermal feedback inputs of both of the lasers through a chain of 16 bit D/A's, Two lasers are locked to two subsequent longitudinal modes of the cavity which are approximately 3 GHz apart. The frequency of both of the lasers can be tuned digitally by ± 13 GHz independently. The maximum tuning range without a laser mode hop is 15 GHz.

Portions of the large power output ports (~ 10 mW) of the lasers are combined to give a beat signal on a wideband photodetector which drives a nine digit frequency counter. The cavity length is determined when both lasers are locked to two subsequent longitudinal modes. The frequency of the beat signal is a direct measure of the cavity length. This number is read out by the servo computer to compute the cavity length to 1 part in 10^7. The main portion of the large power output ports is kept separate and it is fed into the absolute metrology heterodyne modulation system.

Fig. 12 shows the absolute metrology gauge heterodyne modulation system

This system generates two independent heterodyne measurement beams with independent reference detectors using only three acousto-optic modulators. Separate half-wave plates are used to correct any residual polarization rotation on the beams.

Fig. 13 shows the absolute metrology distance measurement system. One of the heterodyne interferometers is used as a linear relative metrology gauge to keep track of the changing distance between the corner cubes while the other one is tuned through its frequency range to determine the absolute distance. The outputs of the measurement

Figure 13: The absolute metrology gauge distance measurement system

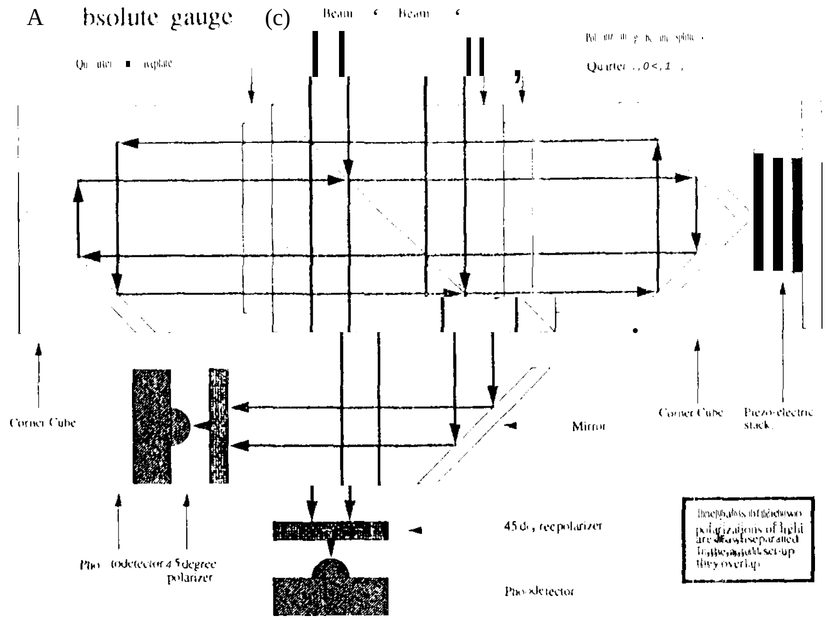

photodetectors are compared to the outputs of the reference photodetectors by the separate metrology CPU to determine the distance and to apply corrections.

Since the initial accuracy of the absolute metrology gauge is 10 microns at 10 meters or equivalently 1 micron at 1 meter, the relative and the absolute measurement beams do not need to overlap. A piezo-electric transducer on one of the corner cubes aids the relative metrology gauge to hold the measurement distance constant by servo action.

3,2. Laser Stabilization Technique

The principle behind the laser stabilization technique is illustrated in Fig. 14. The familiar reflected intensity derived, chopper stabilization system is used. The laser frequency is made to hop to either side of the cavity fringe and an intensity measurement is taken at each side. The difference in these measurements indicate how far the laser frequency is away from the true resonance. A servo signal is generated and applied to the laser to hold the frequency at the right value.

The details of the modulation system is illustrated in Fig. 15. The servo signals are derived and filtered digitally to form the integrators shown in the diagram.

3.3. The Measurement Technique

The measurement of the absolute distance is performed by tuning the absolute distance measurement laser while monitoring the fringe counter output of the corresponding heterodyne interferometer. If the frequency is tuned by an amount F and N fringes passed while the laser is being tuned, the absolute distance D is given by $D = cN/F$ where c is the speed of light This technique is illustrated in Fig. 16 .

The amount of tuning is determined by the number of cavity modes the laser frequency goes through during the tuning. Initially the laser is locked to a particular cavity mode. The locking is released and the laser is tuned an amount which spans several cavity modes. At the end of the tuning, the laser is again locked to the nearest main cavity mode. The tuning amount obtained is an exact multiple of the cavity free spectral range which is independently measured by the laser stabilization system to 1 part in 10^7.

Figure 14: The stabilization method

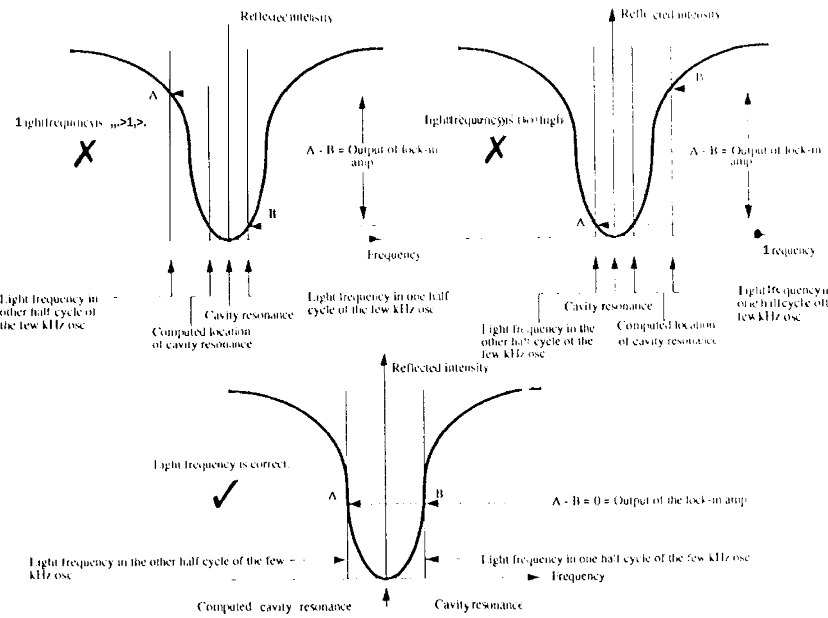

Figure 15: The laser stabilization servo

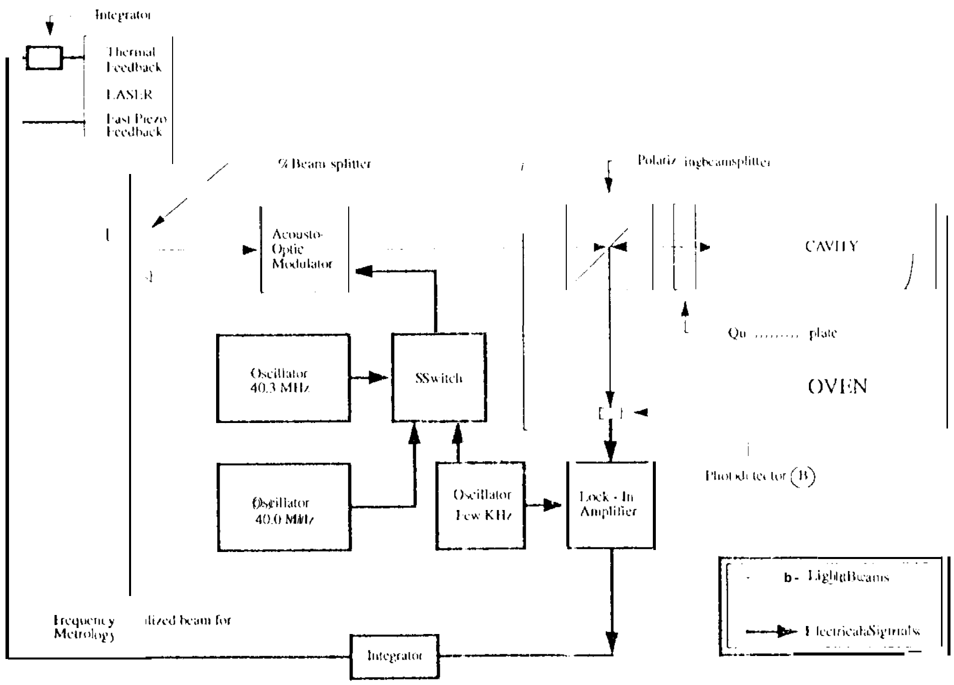

Figure 16: The absolute metrology measurement technique

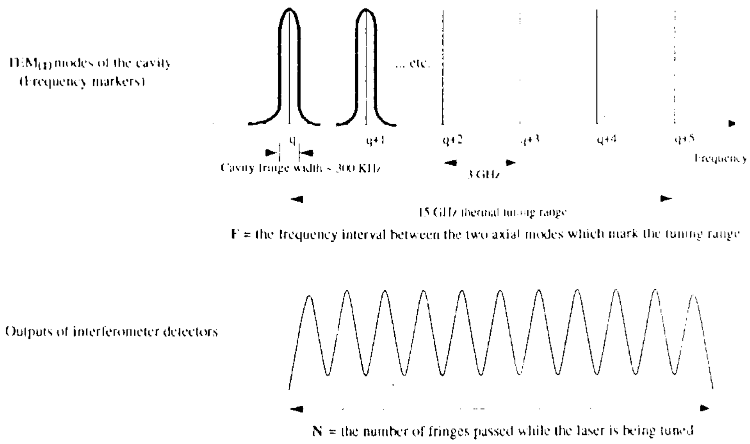

Then, the absolute length D is given by:

$$\boxed{D = c N / F}$$

where c is the speed of light

The number of fringes which passed by is determined by the heterodyne metrology fringe counter system which counts integer as well as fractional fringes. The instantaneous fractional accuracy of the fringe counter system is $\lambda/5120$. Integration of the resulting counts improves this accuracy.

3.4, Performance of Gauge Subsystems

As shown in previous papers, the linear relative metrology part of the gauge is capable of an accuracy of 0.15 pm rms. The same modulation scheme, the same distance measuring architecture and the same fringe counter are used in the absolute metrology gauge.

The following figures illustrate the performance of remaining gauge subsystems. The complete gauge will be operational early this summer.

Fig. 17 shows the cavity temperature servo performance. The plot shows the actual cavity temperature as read by a sensor mounted on the cavity.

Fig. 18 shows main cavity mode fringe as digitally scanned by the stabilization system. The demodulator output is shown. Note that the fringe width is almost exactly 300 kHz.

The figures Fig. 19, Fig. 20, Fig. 21 snow the performance of the laser servo during a **four** day continuous run. The laser was locked to the same cavity fringe at all times. It is capable of **t**racking the length of the cavity with an Allen deviation of few hundred Hertz for a time scale of a day.

Fig. 22 shows the bandwidth of the servo system. The servo gain is raised until the servo starts oscillating. This oscillation occurs when the closed loop gain is nearly unity. The oscillation is recorded while the laser is locked to the fringe by the servo recording system,

Fig. 23 shows the wide range tracking ability of the laser stabilization servo. The cavity thermal servo was turned off for a day to bring the cavity to ambient temperature. The laser was then locked to the cavity and the cavity heater servo was turned on. The laser successfully tracked the lengthening cavity resulting in an upper bound for the expansion coefficient cavity-oven assembly. The run length is too short to determine the exact expansion coefficient.

An initial measurement of the cavity length has been performed using the system described above shortly after

Figure 17: The cavity temperature stability

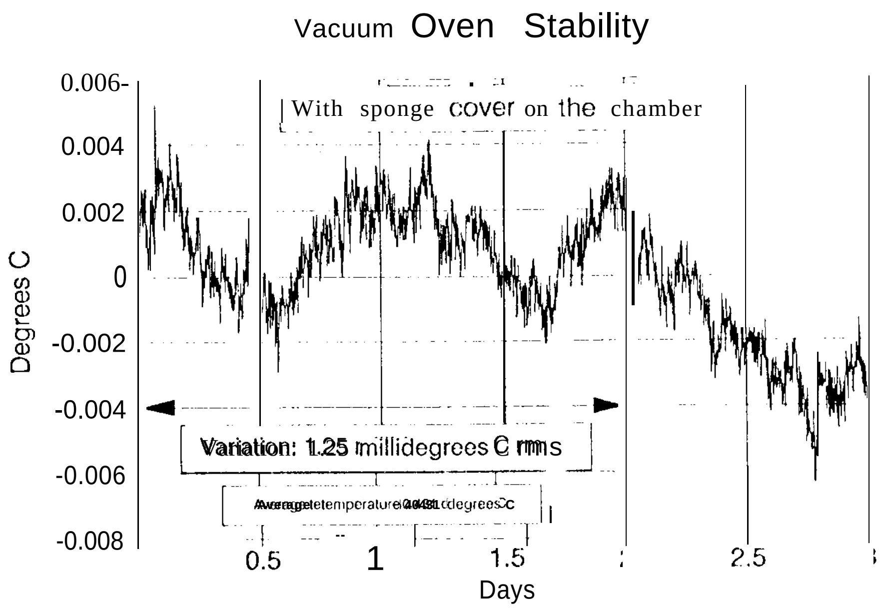

Figure 18: The main cavity mode

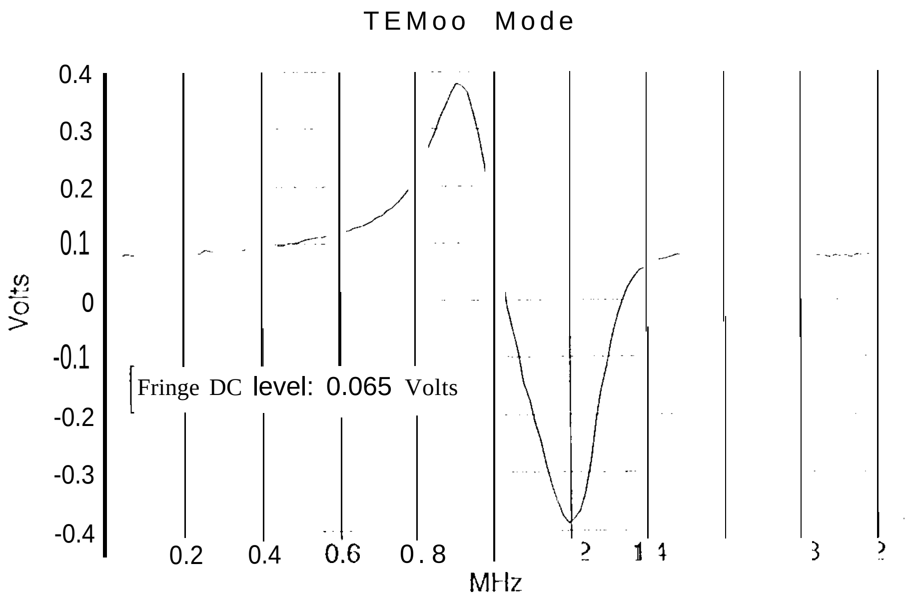

Figure 19: The laser servo performance (a)

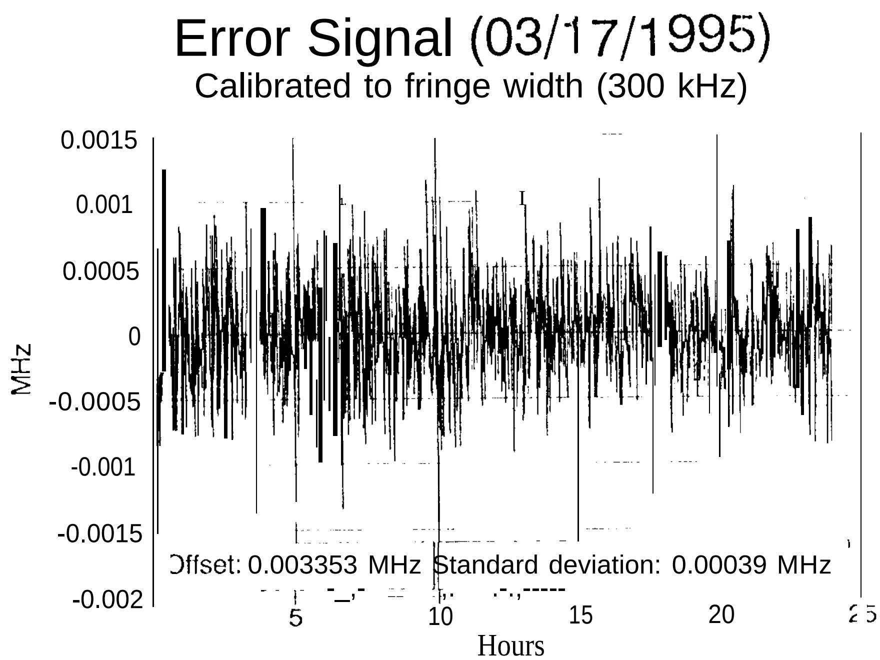

Figure 20: The laser servo performance (b)

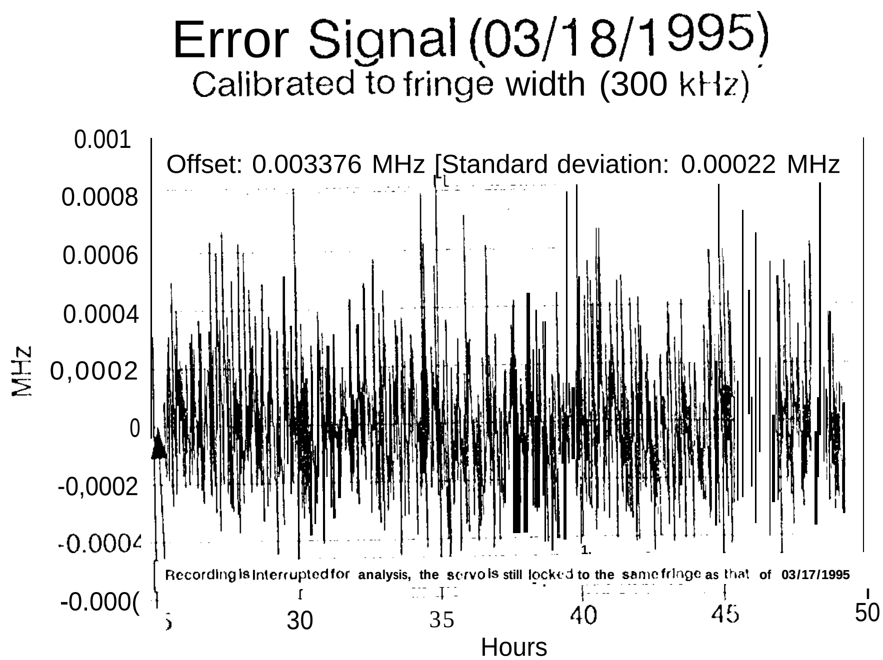

Figure 21: The laser servo performance (c)

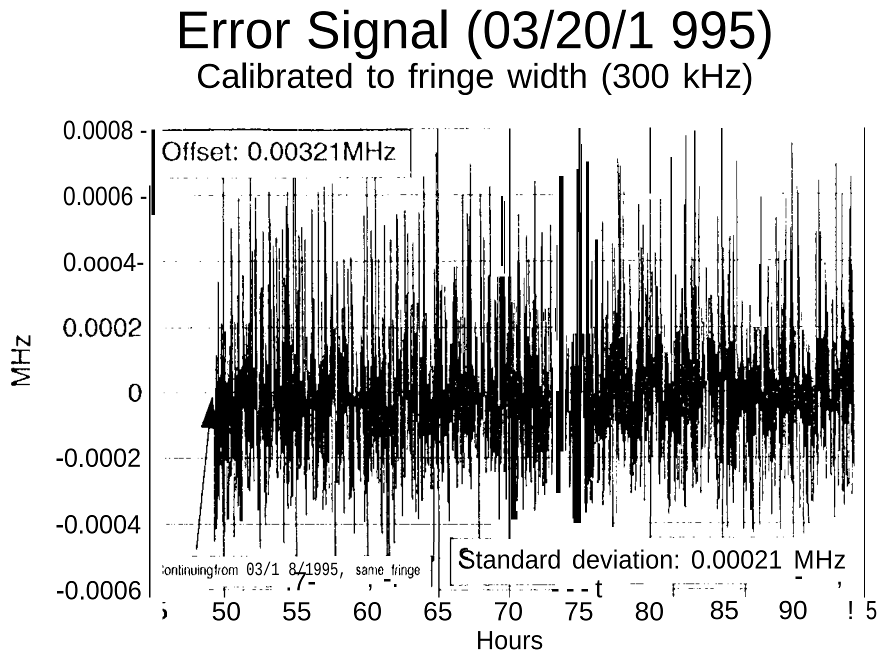

Figure 22: The laser servo bandwidth

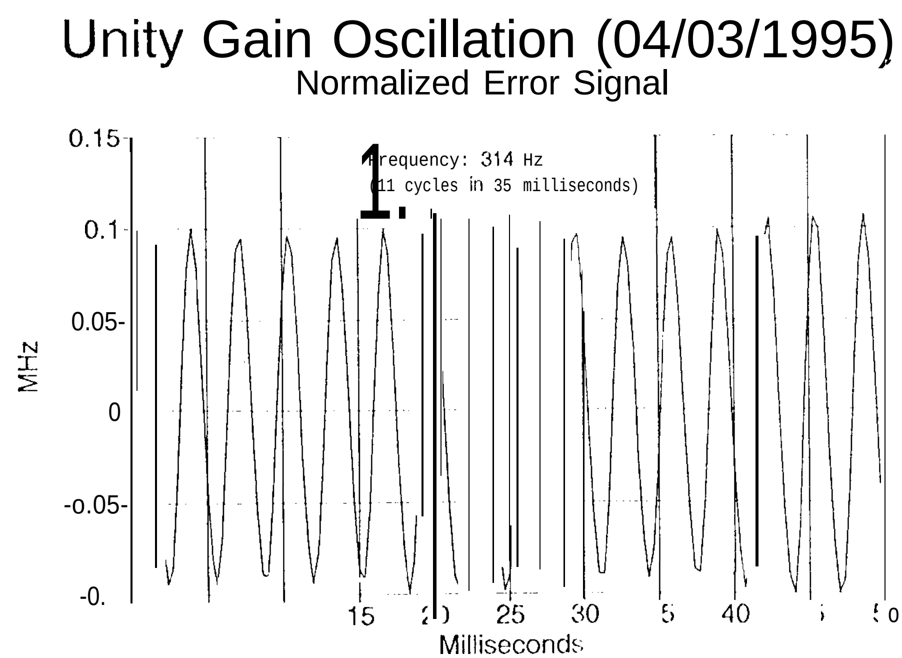

Figure 23: The laser servo wide-range tracking

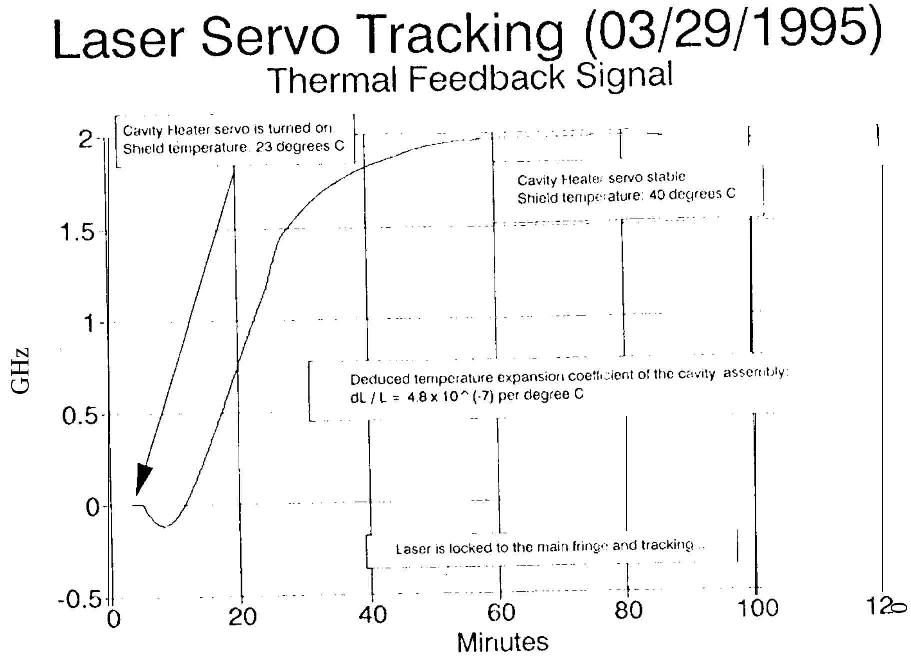

the conclusion of this conference. An accuracy 1 part in 10^6 is obtained with the first data. This result is expected to improve by a factor of 10 rapidly.

4. 3-D METROLOGY GAUGE

The design for the 3-dimensional metrology gauge is presented in the figures Fig. 24, Fig. 25, and Fig. 26. Five linear metrology heads with built in dithering are mounted on a 2' by 2' super invar breadboard which serves as a reference surface. These heads monitor the distance between their internal corner cubes and one external corner cube. The external corner cube is mounted on a five degree of freedom stage to simulate the angles of incidence encountered under realistic conditions.

The design uses the linear relative metrology gauge which was developed before. The improvements to the linear gauge include an all-fiber distribution system and built-in dithering on a thermally stable base. The modulation system remains unchanged. The entire gauge once again is constructed on a seismically isolated optical breadboard inside the four feet vacuum chamber.

The purpose of the gauge is to locate the corner of the external cube with an accuracy of less than 10 pm rms for a measurement time of few minutes. Early results from this gauge will be available late summer and they will be presented in a subsequent paper.

5. SUMMARY

The surface metrology gauge for the Orbiting Stellar Interferometer (OSI has reached a repeatability of less than 0.1 nm. The absolute calibration of the gauge is in progress.

All subsystems of the absolute metrology gauge are functioning within their specifications. The complete gauge will be tested early this summer.

The design for the 3-dimensional metrology gauge is presented. Initial results from this gauge will be available early this fall.

Figure 24: The 3-D metrology configuration

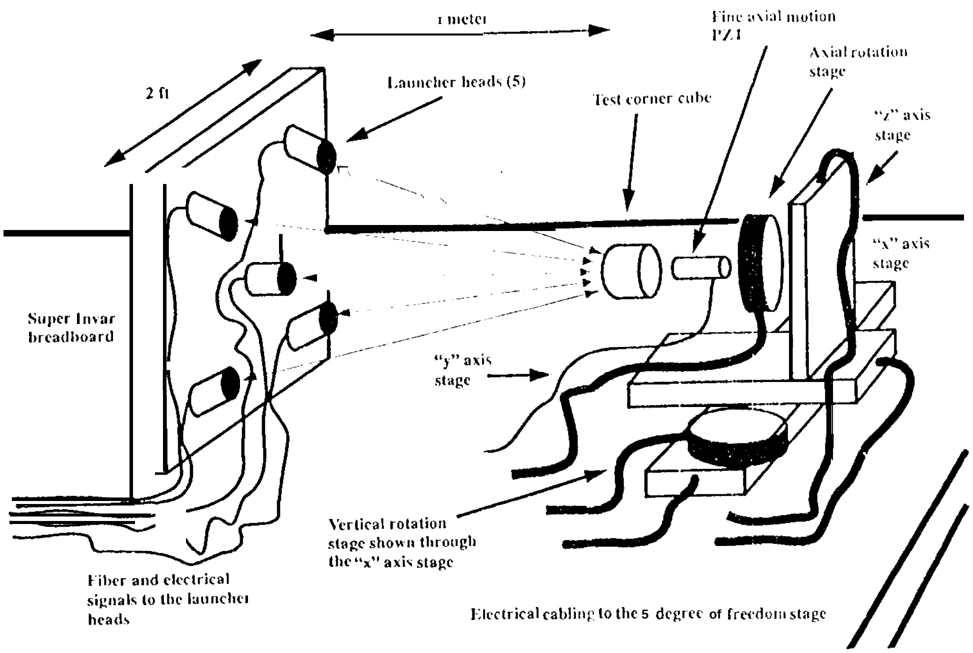

Figure 25: The 3-D metrology launching head

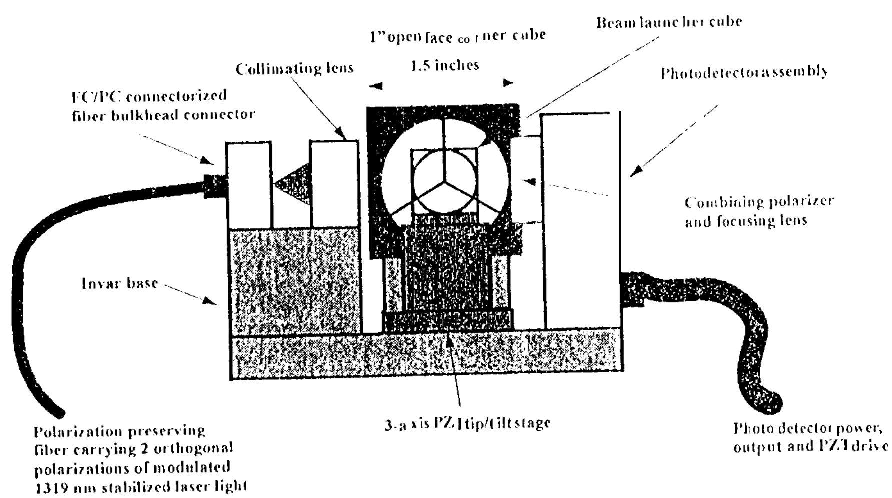

Figure 26: The 3-D metrology modulation subsystem

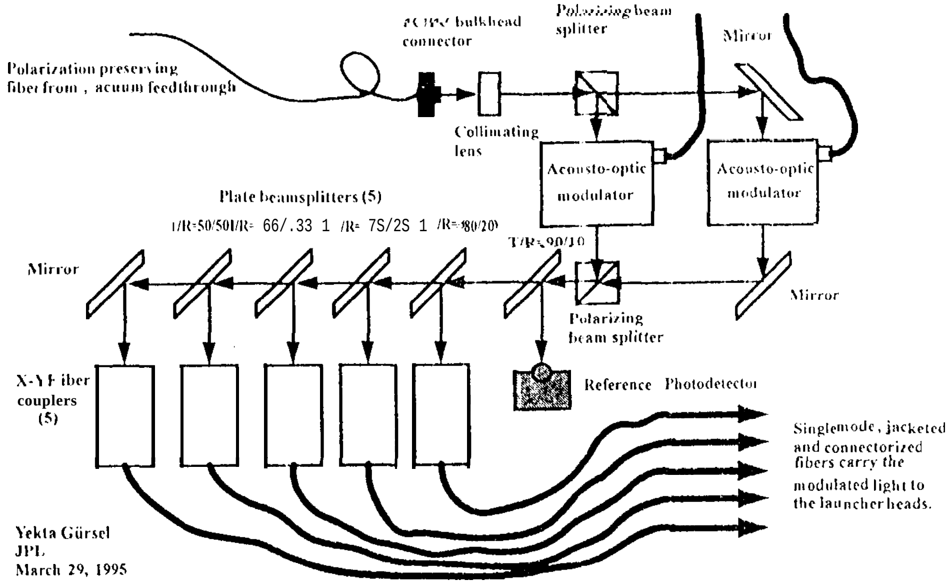

6. ACKNOWLEDGEMENTS

I would like to thank M. Shao and J. Yu for many fruitful discussions. The research described was performed at the Jet Propulsion Laboratory, California Institute of Technology, under a contract with the National Aeronautics and Space Administration.

7. REFERENCES

1. Y. Gürsel. Laser metrology gauges for OSI, *in Proceedings of SPIE conference on Spaceborne Interferometry*, Vol. 1947, p. 188-197, 1993.

2. Y. Gürsel. Metrology for spatial interferometry, *in Proceedings of SPIE conference on Amplitude and Intensity Spatial Interferometry*, Vol. 2200, p. 27-34, 1994.